

Article

A Novel Electrochemical Sensing Platform for the Detection of the Antidepressant Drug, Venlafaxine, in Water and Biological Specimens

Sundas Sultan¹, Afzal Shah^{1,*} , Naveeda Firdous¹, Jan Nisar², Muhammad Naem Ashiq³ and Iltaf Shah⁴ ¹ Department of Chemistry, Quaid-i-Azam University, Islamabad 45320, Pakistan² National Centre of Excellence in Physical Chemistry, University of Peshawar, Peshawar 25120, Pakistan³ Institute of Chemical Sciences, Bahauddin Zakaryia University, Multan 6100, Pakistan⁴ Department of Chemistry, College of Science, United Arab Emirates University, Al Ain P.O. Box 15551, United Arab Emirates

* Correspondence: afzalshah@qau.edu.pk or afzals_au@yahoo.com

Abstract: A stable bimetallic catalyst composed of Co–Pd@Al₂O₃ was synthesized using a wet impregnation method, followed by calcination and H₂ reduction. The synthesized catalyst was thoroughly characterized using XRD, BET, SEM, EDX, and TPR techniques. The catalyst was then drop-casted on a glassy carbon electrode (Co–Pd@Al₂O₃/GCE) and applied for the sensitive and selective electrochemical determination of a common antidepressant drug, venlafaxine (VEN). The proposed sensor (Co–Pd@Al₂O₃/GCE) demonstrated a remarkable catalytic activity for the electro-oxidation of VEN, with a decent repeatability and reproducibility. The pH dependent responsiveness of the electro-oxidation of VEN helped in proposing the redox mechanism. A linear relationship between the peak current and concentration of VEN was observed in the range of 1.95 nM to 0.5 μM, with LOD and LOQ of 1.86 pM and 6.20 pM, respectively. The designed sensor demonstrated an adequate selectivity and significant stability. Moreover, the sensor was found to be quite promising for determining the VEN in biological specimens.

Keywords: electrochemical sensor; venlafaxine detection; electrochemical oxidation; limit of detection; biological specimens



Citation: Sultan, S.; Shah, A.; Firdous, N.; Nisar, J.; Ashiq, M.N.; Shah, I. A Novel Electrochemical Sensing Platform for the Detection of the Antidepressant Drug, Venlafaxine, in Water and Biological Specimens. *Chemosensors* **2022**, *10*, 400. <https://doi.org/10.3390/chemosensors10100400>

Academic Editor:
Dario Compagnone

Received: 27 August 2022
Accepted: 30 September 2022
Published: 4 October 2022

Publisher's Note: MDPI stays neutral with regard to jurisdictional claims in published maps and institutional affiliations.



Copyright: © 2022 by the authors. Licensee MDPI, Basel, Switzerland. This article is an open access article distributed under the terms and conditions of the Creative Commons Attribution (CC BY) license (<https://creativecommons.org/licenses/by/4.0/>).

1. Introduction

Venlafaxine (VEN), chemically known as 1-[2-(dimethylamino)-1-(4-methoxyphenyl)ethyl] cyclohexanol, is a member of a class of drugs known as selective serotonin and norepinephrine reuptake inhibitors (SSNRIs). It is extensively prescribed as an antidepressant to adults and children with nightmares, cataplexy, and narcolepsy [1]. The commonly recommended dosage of VEN ranges from 75 to 375 mgs per day. Over dosages may lead to cardiac arrhythmias, serotonin syndrome, depression, coma, hypertension, or hypotension, and may even cause death [2]. Thus, assessment of the toxicity, interactions, and remedial proficiency, as well as observation of the level of the drug in bio fluid, has become clinically and medically necessary [3]. A survey of the literature has revealed chromatography to be a leading technique for the trace level sensing of VEN [4–10]. The broadly used approaches for VEN studies in bio-specimens include high-performance liquid chromatography (HPLC), along with ultraviolet detection [11,12], liquid chromatography/mass spectrometry (LC/MS) [13], gas chromatography (GC) [14], solid-phase extraction [15], capillary electrophoresis [16], and electrochemical methods [17–20]. Although chromatographic approaches are quite sensitive and proficient, these approaches are quite time-consuming and thus cannot be used for efficient drug analysis [21]. Furthermore, chromatographic approaches have a higher on-column packing of the analytes at the LOQ level, which might decrease the column efficiency and shorten the lifetime of the column.

In contrast, electro-analytical methods are very efficient, sensitive, and selective, and do not require any pre-treatment or any type of pre-separation [22,23]. The accessibility of several chemically fabricated electrodes at a comparatively lower cost provides a significant incentive for the determination of drug molecules using electroanalytical techniques. Thus, we took interest in developing a somewhat simple, sensitive, and accurate alternate scheme for the determination of VEN.

The modification of electrode surfaces plays a great role in electron transfer kinetics and electrocatalytic studies. Modified electrodes are widely applied in electrocatalytic studies, electrochemical devices, energy conversion, and chemical analysis [24]. Electrode modification with metal nanoparticles (NPs) has presented an excellent electrochemical activity owing to the optimum surface area, maximum metal dispersion, controlled morphology, excellent durability, chemical inertness, and good conductive properties [25–27]. In addition, the preparation of electrochemical sensors by modifying the electrode surface with NPs has been of great interest for the sensing of trace amount of analytes, which can be attributed to the amplification of electrochemical signals, leading to ultrasensitive assessments. NP-based electrochemical sensors have been developed either through the direct use of NPs as electroactive species or in the form of semiconductors to enhance electrochemical detection [28,29]. NPs are deposited on the electrode surface in order to load the electroactive species for improving the detection limit of molecules [30–33]. In this scenario, the modification of electrode surfaces with metal catalysts has shown an excellent electroactivity. Metal NPs are highly beneficial for electrocatalytic studies due to their high surface area, maximum metal dispersion, controlled particle size, morphology of the attached nanoparticles, good electrical characteristics, and stability [34,35]. The synergy of two metals in bimetallic catalysts sometimes results in a better activity, good electrical conductance, excellent stability, and better mass/electron transfer properties [36,37]. Among the various supports, gamma alumina (γ - Al_2O_3) offers a large surface area, mesoporous character, narrow pore-size distribution, and good mechanical characteristics [38]. The oxide groups of alumina have a proton-donating nature. Hence, alumina-coated glassy carbon electrodes (GCE) can overcome the overpotential and improve the sensitivity of many materials [39,40]. The modified electrodes with metal NPs such as Pd-Ni/C [41], Au/C [42–45], Ni/graphite [46,47], and Pt-Co/CNT [48] are widely used for various electrochemical applications. In recent years, most studies have focused on VEN electrochemical sensing using various metal oxides [49–52], whereas metal NP-based electrochemical sensors for VEN studies are rather scarce. Hence, in the current article, we report the synthesis of Co-Pd@ Al_2O_3 bimetallic catalysts and their deposition on GCE for designing a voltammetric sensor to detect venlafaxine in human serum samples. To the best of our knowledge, no previous reports have been carried out on the quantitation of venlafaxine using a Co-Pd@ Al_2O_3 bimetallic catalyst. The designed sensing platform presented an excellent performance towards venlafaxine oxidation, with a wide linear range and low detection limit, which might be due to the high electrical conductivity and synergistic effect of the bimetallic NPs.

2. Experiment

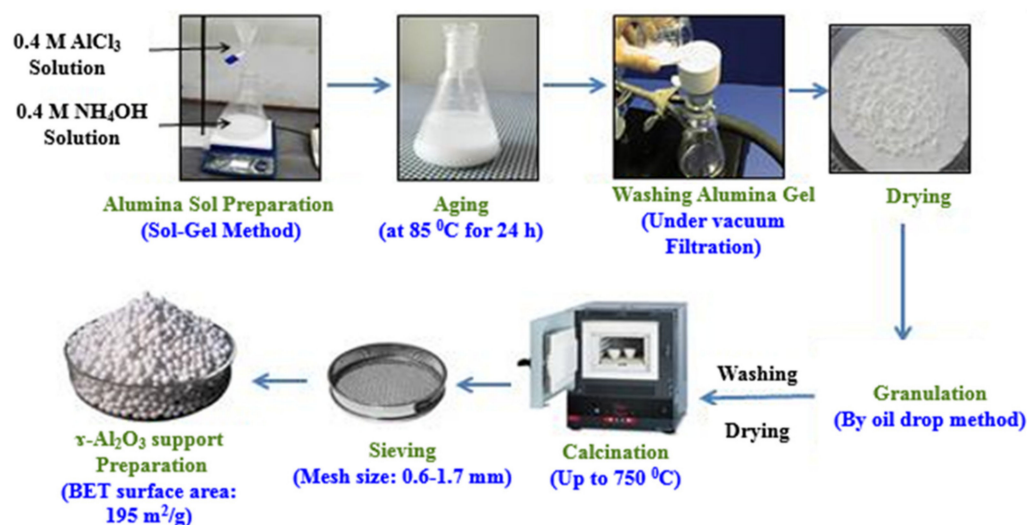
2.1. Reagent and Apparatus

Electrochemical studies were carried out on a Metrohm Autolab PGSTAT302N (Herisau, Switzerland) using NOVA 1.11 and FRA software. The conventional three-electrode system was used for electrochemical testing. A bare and modified glassy carbon electrode was used as a working electrode, Ag/AgCl (3M KCl) as a reference electrode, and Pt wire as a counter electrode. pH measurements were carried out using the INOLAB pH meter.

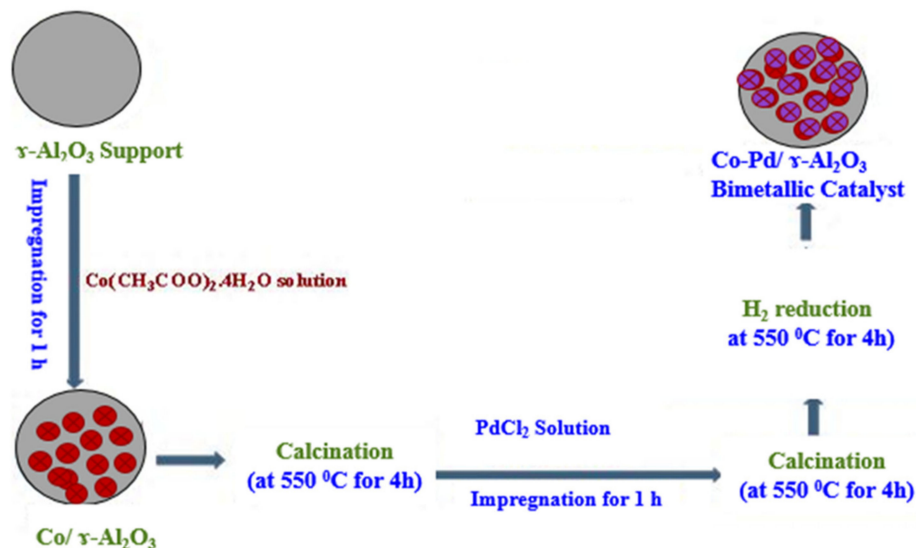
Venlafaxine hydrochloride (Fluka), cobalt acetate tetrahydrate ($\text{Co}(\text{C}_2\text{H}_3\text{O}_2)_2 \cdot 4\text{H}_2\text{O}$, Aldrich, 99.9%), and palladium chloride (PdCl_2 , Aldrich, 99%) were used as received, without any purification. Al_2O_3 powder and Nafion were purchased from Sinopharm Chemical Reagent Co., Ltd., (Shanghai, China). Deionized water was used in the preparation of all aqueous solutions.

2.2. Catalyst Preparation

The alumina support was prepared using the precipitation method, as described earlier [53] and as shown in Scheme 1. After calcination at 550 °C for 3 h, alumina was ground finely into a fine powder form. The Co–Pd@Al₂O₃ bimetallic catalyst was prepared via the impregnation method with a total metal loading of 10 wt%, as presented in Scheme 2. For this purpose, Al₂O₃ powder was mixed with the aqueous solution of cobalt acetate and palladium chloride. The concentration of both metal precursors was adjusted to obtain the desired metal loading of the catalyst. The solution was stirred continuously for 5 h at 25 °C for thorough metal loading. Then, the suspension was concentrated under vacuum conditions. Finally, the H₂ reduction of the catalyst was conducted at 550 °C for 4 h.



Scheme 1. Preparation of the γ -Al₂O₃ support.



Scheme 2. Preparation of the Co–Pd/ γ -Al₂O₃ catalyst using the wet impregnation method.

2.3. Electrode Modification

First, the GCE surface was thoroughly cleaned. The modification of bare GCE was performed by coating Co–Pd@Al₂O₃ NPs according to the following procedure: 1 mg of catalyst powder was dispersed in 5 μ L ethanol via ultra-sonication for 20 min. Then, 5 μ L of the prepared suspension was drop-casted onto the electrodes, followed by two to three drops of Nafion solution. The modified electrode was ready for use after being completely dried at room temperature.

2.4. Characterization

The elemental analysis was performed by the atomic absorption spectrophotometry (AAS) technique by running the samples on the Perkin Elmer AA400. X-ray powder diffraction (XRD) analysis was performed on an analytical diffractometer (Rigaku D/Max 2500) with a graphite monochromatic radiation source Cu K α 1 ($\lambda = 1.54056 \text{ \AA}$). The morphology of the catalyst was examined using a scanning electron microscope (SEM) (MIRA3, TESCAN) equipped with an EDX (energy dispersive spectroscopy) unit for the chemical analysis. The surface area analysis was measured on the basis of the BET (Brunauer, Emmett, and Teller) method by using the Sorptometer Kelvin 1042 instrument after degassing the sample at 120 °C for 1 h.

3. Results and Discussion

Elemental analysis of the synthesized catalyst by AAS revealed a Co metal content of 14.11 wt% and Pd content of 5.82 wt%. These results were found to be in good agreement with the theoretical metal loadings (Co = 15 wt%, Pd = 5 wt%), thus presenting an effective procedure for catalyst preparation.

Moreover, EDX analysis was conducted to ensure the elemental composition of the catalyst. Figure 1a shows the EDX spectrum, in which the co-existence of Co and Pd metals ensured the formation of Co–Pd alloy NPs. The EDX analysis of the prepared catalyst detected Co = 13.34 wt%, Pd = 4.74 wt%, O = 47.97 wt%, and Al = 33.95 wt%. The EDX composition was found to be close to the AAS results, thus confirming the metallic stoichiometric contents. The surface morphology of the prepared Co–Pd nanoparticles dispersed on alumina was analyzed by SEM. The SEM image (Figure 1b) of the prepared catalyst presented the formation of spherical Co–Pd alloy NPs. The metal particles were found uniformly distributed over the surface of the Al₂O₃. The size of the bimetallic NPs varied, ranging from 45 to 85 nm. In addition, EDX mapping was recorded (Figure 1c), where the uniform distribution of the metal NPs was observed over the alumina support.

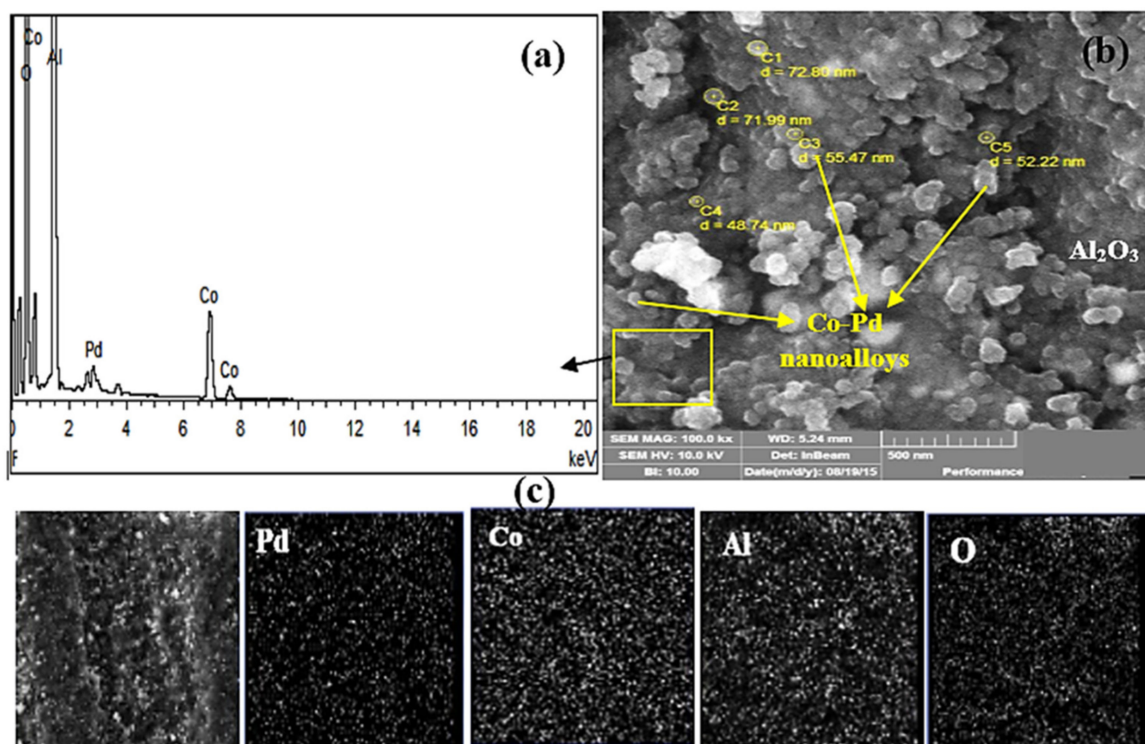


Figure 1. (a) EDX profile, (b) SEM image, and (c) EDX mapping of the synthesized Co–Pd@Al₂O₃ bimetallic catalyst.

The XRD analysis was conducted to study the crystalline features of the prepared sample. Figure 2 presents the XRD profile of the Co–Pd@Al₂O₃ catalyst. The significant peaks appeared at 37.3°, 45.7°, and 67.1°, corresponding to the hkl values of (311), (400), and (440), respectively. These values are consistent with the standard pattern of Al₂O₃ (ICDD card no. 00-001-1303), showing a cubic crystal structure. Moreover, two additional broad peaks appeared at 32.9° and 59.6°, which were consistent with the standard pattern of Co (JCPDS:15-0806), with hkl values of (210) and (411), respectively. Small peaks were noticed at 39.2° and 55.7° for the Pd metal, which may either be due to its low content or the metal particles being too small, with corresponding hkl plans of (111) and (200), matching the reference card (JCPDS: 46-1043). Broad diffraction peaks showed the nanosized nature of the product, with an average crystallite size of 18 nm, as computed by the Debye–Scherrer formula.

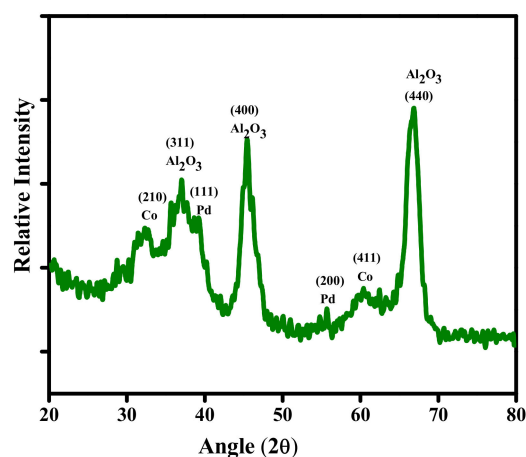


Figure 2. XRD pattern of the prepared Co–Pd@Al₂O₃ bimetallic catalyst.

Figure 3a presents the adsorption–desorption isotherms of Co–Pd/Al₂O₃ with a type IV hysteresis loop, which represented the mesoporous nature of the material [54–56]. The BET area of the catalysts was found to be 112 m² g^{−1}, which was much lower than Al₂O₃ (205 m² g^{−1}). The decrease in the BET area can be related to the filling of Al₂O₃ pores with metal particles as well as the sintering process. Figure 3b presents the distribution of pores in a narrow range with a maximum pore size of 3.3 nm in diameter.

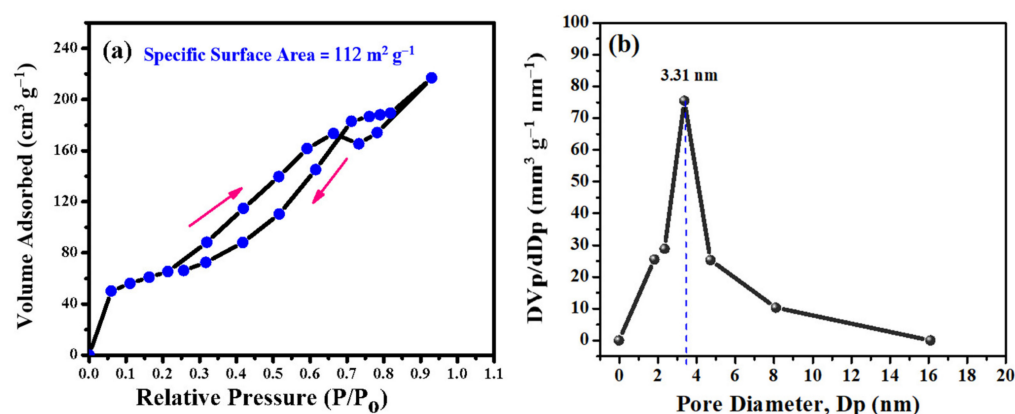


Figure 3. (a) N₂ adsorption–desorption isotherm and (b) pore size distribution plot of the Co–Pd@Al₂O₃ bimetallic catalyst.

Temperature programmed reduction (TPR) measurements were performed to study the reduction behavior of metal alloy NPs in bimetallic systems. Figure 4 presents the TPR profile of the Co–Pd@Al₂O₃ bimetallic catalyst. The Co/Al₂O₃ monometallic catalyst had a strong interaction with the Al₂O₃ support, and therefore showed reduction peaks in the high-temperature region. Upon the incorporation of Pd metal, the reduction peaks were

shifted towards a lower temperature region. The alloying of Pd and Co metals resulted in an improvement in the catalytic activity that could be related to an easing of reducibility, better metal dispersion, and smaller particle size.

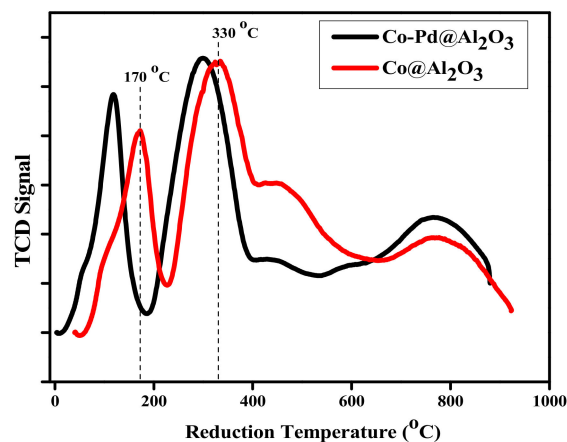


Figure 4. TPR profile of the prepared catalysts.

3.1. Electrochemical Characterization

The proficient electron transfer capability of Co–Pd@Al₂O₃-modified GCE was verified in the electrochemical impedance spectroscopy (EIS) studies using a 5.0 mM solution of K₃[Fe(CN)₆] in 1.0 M KCl solution. The Nyquist plots are shown in Figure 5, the data of which have been analyzed and fitted using the analogous Randles circuit (displayed in the inset). R_s is the electrolyte resistance, R_{ct} is the charge (electron) transfer resistance, and W is the Warburg impedance. A semicircle at a higher frequency is linked with an interfacial charge transfer process and its diameter refers to the charge transfer resistance (R_{ct}), while the linear part at lower frequency is related to diffusion processes [57,58]. R_{ct} values for bare GCE and modified GCE were recorded as 6.41 k Ω and 3.33 k Ω , respectively. The decrease in R_{ct} values suggests an enhancement in the charge transfer process for Co–Pd@Al₂O₃-modified GCE.

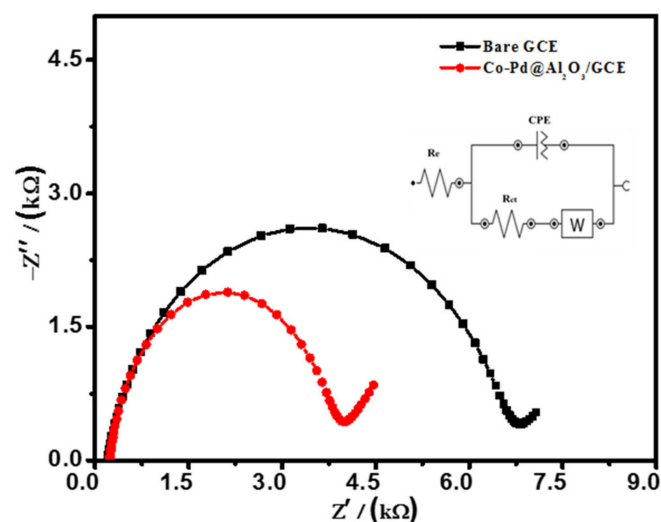


Figure 5. Nyquist plots for bare GCE and Co–Pd@Al₂O₃/GCE in the 5 mM solution of the redox probe K₃[Fe(CN)₆].

The electron transfer process of Co–Pd@Al₂O₃-modified GCE was also studied by cyclic voltammetry (CV) using a 0.1 M KCl solution containing 5.0 mM K₃[Fe(CN)₆] as a model redox couple at a scan rate of mV s^{−1}. Figure 6 presents the cyclic voltammograms with a reasonably reversible redox behavior. For Co–Pd@Al₂O₃-modified GCE,

the sharp peak current with a narrow peak potential difference and an obvious enhancement in the oxidation–reduction was observed in comparison with bare GCE, signifying a rapid electron transfer process. In order to demonstrate that Co–Pd@Al₂O₃ improves the surface area and conductivity of the electrode, the Randles–Sevcik equation was used ($I_p = 2.6 \times 10^5 n^{3/2} D^{1/2} \nu^{1/2} AC$). The surface area was calculated to be 0.02 and 0.04 cm² for bare GCE and Co–Pd@Al₂O₃-modified GCE, respectively. A two-fold increase in the surface area compared with the unmodified electrode led to an enhanced current intensity of the redox probe.

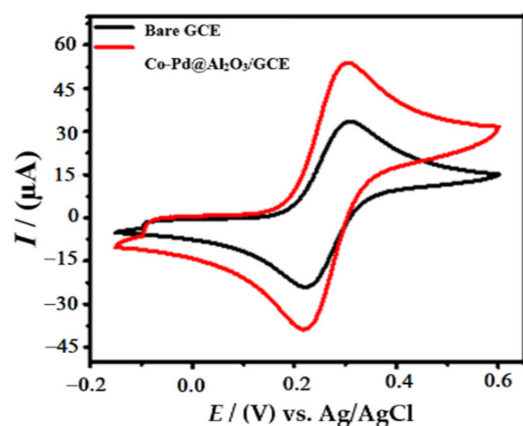


Figure 6. Cyclic voltammograms at bare GCE and Co–Pd@Al₂O₃/GCE in a 5 mM solution of K₃[Fe(CN)₆] in 0.1 M KCl.

Square Wave Anodic Stripping Voltammetric Analysis of the Targeted Analyte

By using SWASV, an electro-oxidation response of VEN was obtained at a potential of 0.65 V, as presented in Figure 7. A clearly enhanced current response for the electro-oxidation of VEN was obtained at Co–Pd@Al₂O₃/GCE compared with the bare GCE. This much boosted current response can be ascribed to the decent conductivity of Co–Pd@Al₂O₃/GCE towards the facile oxidation of VEN oxidation. An observation of Figure 6 reveals that the active surface area increased two times, while Figure 7 shows that the peak current of the analyte at the modified electrode increased by about three times compared with the bare electrode. Hence, the higher surface area of the modified electrode accompanied with the catalytic role of the modifier is responsible for the peak current amplification. The obtained outcomes confirmed that the proposed sensor is a suitable platform for VEN detection.

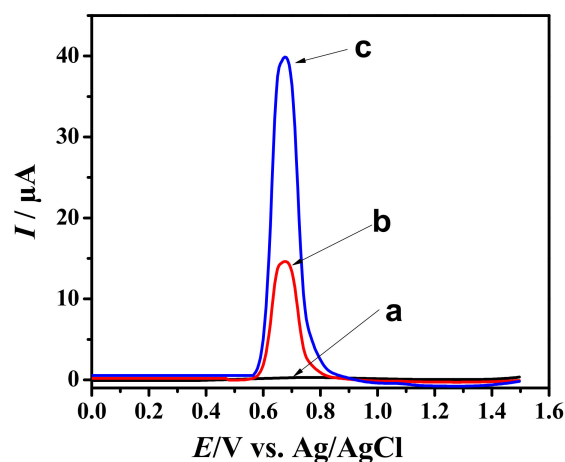


Figure 7. (a) Blank voltammogram obtained at Co–Pd@Al₂O₃/GCE is for the buffered medium (BRB solution of pH of 7), (b) voltammogram of the 2 μM solution of VEN in BRB of pH 7 at bare GCE, (c) voltammogram of the 2 μM solution of VEN in BRB of pH 7 at Co–Pd@Al₂O₃/GCE. Conditions: scan rate of 50 mV/s; deposition potential of –0.5 V; deposition time of 60 s.

3.2. Optimization of the Experimental Parameters

3.2.1. Influence of the Supporting Electrolyte and pH

The effects of several buffer solutions, including the Britton–Robinson buffer with a pH ranging from 6 to 11, acetate buffer solution, and phosphate buffer solutions, were studied. Among the selected buffer solutions, BRB produced the finest response in terms of a higher peak current signal and well-defined peaks for the oxidation of VEN. The pH effect on the oxidation peak current of VEN on the Co–Pd@Al₂O₃/GCE was also studied at a pH ranging from 6 to 11. The best current signal was found at a pH of 7, as shown in Figure 8A.

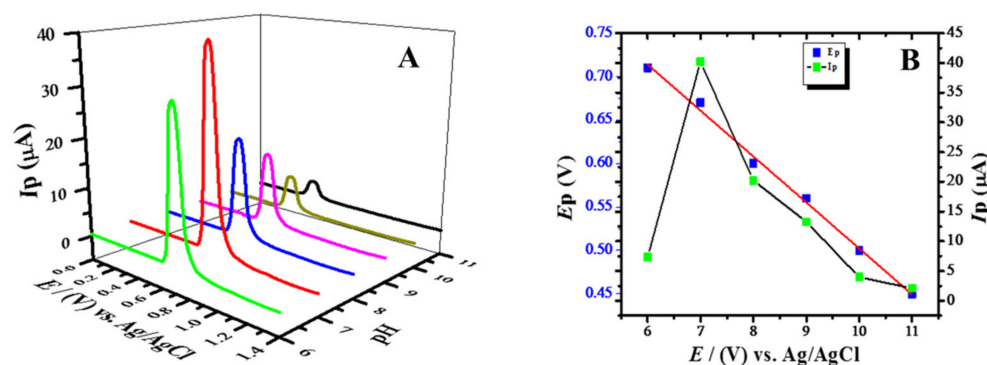
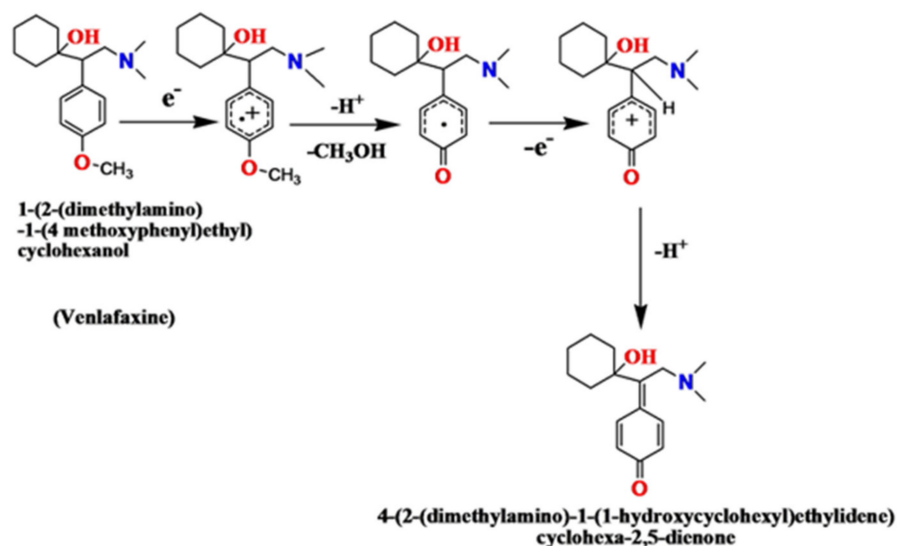


Figure 8. (A) Square wave voltammograms of the 2 μM solution of VEN in media of different pH obtained at a scan rate of 50 mV/s, accumulation potential of -0.5 V, and accumulation time of 60 s. (B) Plots of the peak potentials and peak currents versus pH.

As shown in Figure 8B, by increasing the pH, the peak shifted toward a more negative potential. As the Nernstian dependency of the peak potential on the pH was observed and the electrooxidation of VEN is well known to involve a two-electron transfer [33], the number of involved protons could be estimated as two, which is consistent with the following proposed mechanism (Scheme 3).



Scheme 3. Proposed mechanism of the oxidation of VEN at the Co–Pd@Al₂O₃/GCE.

3.2.2. Influence of the Deposition Potential and Deposition Time

The effect of the deposition potential and deposition time at I_p of 2 μM VEN was also analyzed via SWASV in order to understand the adsorption process of VEN at the electrode surface. The highest I_p was obtained at a deposition potential of -0.5 V and at a deposition time of 60 s, as shown in Figure 9. Thus, further studies were carried out at this optimized deposition potential and deposition time.

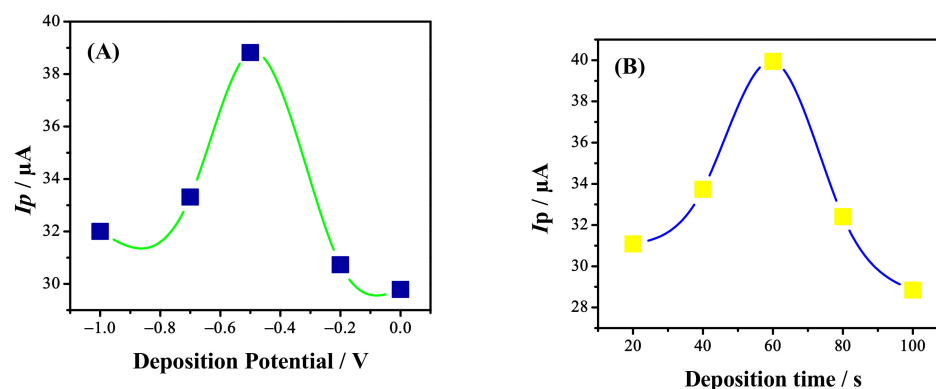


Figure 9. (A) The effect of the deposition potential on the oxidation peak current of VEN, keeping the deposition time constant (60 s), and (B) the effect of the accumulation time on the oxidation peak current maintaining its accumulation potential (-0.5 V) for Co-Pd@Al₂O₃/GCE in the 2 μM solution of INZ by applying the SWASV technique.

3.3. Analytical Characterization

The proposed Co-Pd@Al₂O₃/GCE was used for the determination of various concentrations of VEN in order to find the lowest detection limit using SWASV. The voltammograms obtained for the different concentrations of VEN are presented in Figure 10. A linear calibration plot was obtained for a concentration between 1.95 nM and 0.5 μM , as shown in Figure 10 (inset). The calibration plot was then used to determine the limit of detection (LOD = 3 s/m) and the limit of quantification (LOQ = 10 s/m) of VEN. The current values ($n = 11$) of the blank solution at the peak position of VEN were used to compute the standard deviation [48]. The computed detection and quantification limits of VEN were 1.86 pM and 6.20 pM, respectively.

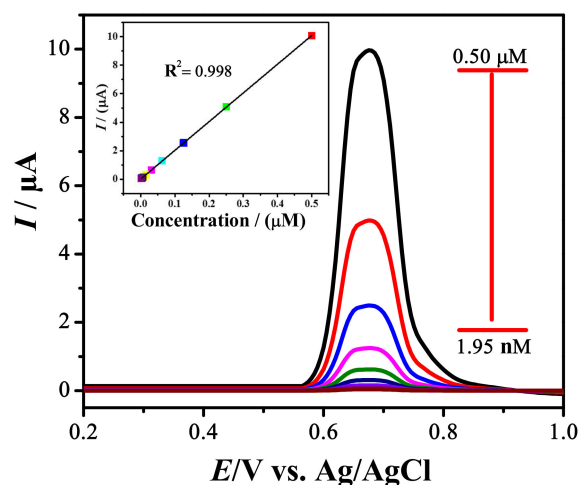


Figure 10. SWAS voltammograms of VEN in the concentration range of 0.5 μM to 1.95 nM at Co-Pd@Al₂O₃/GCE in a BRB solution with a pH of 7 under optimized conditions (scan rate of 50 mV/s, accumulation potential of -0.5 V, and accumulation time of 60 s) and (graph in the inset) the plot of I_{pa} versus the concentration of VEN.

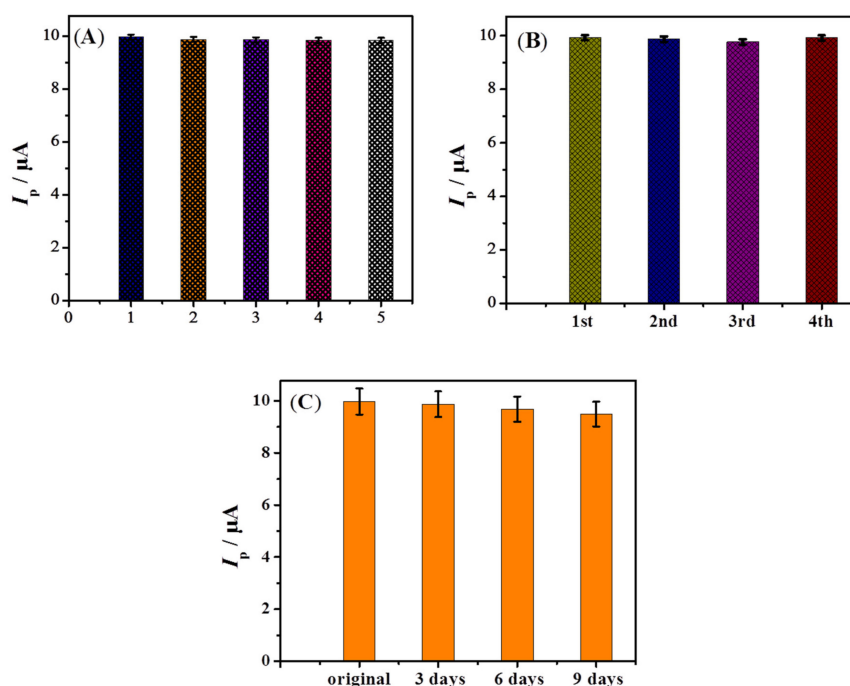
A comparison of the proposed Co-Pd@Al₂O₃/GCE electrode with the previously reported modified electrodes for the determination of VEN is shown in Table 1 [4,49,59–64]. The data show that our designed electrochemical sensor had a lower limit of detection and good linearity range, which are considered to be two important figures of merit for an effective sensing platform. Thus, the proposed sensor was found to be efficient for the detection of VEN.

Table 1. The comparison of the reported detection limits of VEN with this work.

Electrodes	Linearity Range (μM)	Limit of Detection (μM)	References
$\text{La}^{3+}/\text{Co}_3\text{O}_4$ nanocubes/SPE	1–500	0.5	[4]
Eu^{3+} doped NiO/CPE	0.04–300	0.01	[49]
NAF-CNT-GCE	0.038–62.2	0.012	[59]
Mercury film microelectrode	1.27–24.3	0.69	[60]
$\text{Fe}_3\text{O}_4@\text{CNC}/\text{Cu}/\text{GSPE}$	0.05–600	0.01	[61]
MWCNT/CILE/CPE	10–500	0.47	[63]
MWCNT-RTIL/GCE	2–2000	1.69	[64]
$\text{Gd}_2\text{O}_3/\text{SPE}$	5–900	0.21	[52]
Co–Pd@ $\text{Al}_2\text{O}_3/\text{GCE}$	1.95 nM–0.5 μM	1.86 pM	Present work

3.3.1. Repeatability, Stability, and Reproducibility of Co–Pd@ $\text{Al}_2\text{O}_3/\text{GCE}$

The repeatability of the fabricated electrode was examined under the optimized conditions by five successive determination runs of the same Co–Pd@ $\text{Al}_2\text{O}_3/\text{GCE}$ in the BRB with a pH of 7 and the 0.5 μM VEN solution, and at the end of each determination, the current was recorded. The results obtained showed the relative standard deviation (%RSD) in an acceptable range of less than 1%. The reproducibility of the electrode was also examined by employing four separately fabricated electrodes for the detection of 0.5 μM VEN under the same conditions, and the %RSD was found to be in the tolerable range, i.e., below 5%. The stability of the fabricated electrode was inspected for 10 days. The electrode was implied for the SWASV detection of VEN after three days, six days, and nine days. The %RSD was found to be 4%, as also shown in Figure 11. The stability of the fabricated electrode was acceptable during this period. These outcomes indicate that the developed Co–Pd@ $\text{Al}_2\text{O}_3/\text{GCE}$ had a good repeatability, reproducibility, and stability in the synthesis procedure and voltammetric determination of VEN.

**Figure 11.** Current response in the context of (A) repeatability, (B) fabrication reproducibility, and (C) stability of the proposed electrode.

3.3.2. Interference Study

The selectivity of the fabricated GCE electrode was investigated for the determination of VEN, in the presence of potential interfering species that are commonly found in human plasma and pharmaceutical samples. The tolerance limit of these interfering substances was considered as the maximum concentration that gave a %RSD of less than 5% at a 0.5 μM concentration of VEN under optimized conditions. The results obtained showed that the 100-fold excess of citric acid, glucose, ascorbic acid, sucrose, and uric acid had no noteworthy influence on the oxidation peak current of VEN (RSD was found to be less than 5%). The results obtained also displayed excellent recoveries in the range of 95 to 99%, showing that the fabricated GCE electrode had great selectivity for the determination of VEN in biological samples in the presence of the most common interfering species as mentioned in Table 2.

Table 2. Interference study in the presence of various interfering species commonly found in the pharmaceutical preparation of VEN.

Interferents	VEN:Interferents	Recovery% \pm RSD ^a
Citric Acid	1:50	98.7% \pm 0.45
	1:100	99.0% \pm 0.57
Glucose	1:50	98.1% \pm 0.39
	1:100	98.3% \pm 0.35
Ascorbic Acid	1:50	97.1% \pm 0.48
	1:100	98.0% \pm 0.43
Sucrose	1:50	97.9% \pm 0.46
	1:100	98.1% \pm 0.43
Uric Acid	1:50	98.2% \pm 0.49
	1:100	98.7% \pm 0.45

a: average of three readings.

We used the introduced technique to identify VEN in the serum specimens in order to assess its analytical value. The proposed method was employed for the determination of VEN in the test solution, with a known concentration of VEN added to the serum sample, followed by an evaluation of the percentage of recoveries using direct calibration. The recovery percentage of the VEN solution using Co-Pd@Al₂O₃/GCE in the serum samples under optimized conditions can be seen in Table 3.

Table 3. The recovery percentage of the VEN solution using Co-Pd@Al₂O₃/GCE in serum samples.

Sample	Before Addition	Added (μM)	Found (μM)	Recovery (%) \pm RSD
Sample 1	-	0.50	0.490	98.0 \pm 0.48
Sample 2	-	0.25	0.246	98.4 \pm 0.49

4. Conclusions

Co-Pd@Al₂O₃ was employed for the first time as a modifier of the GCE surface. In an aqueous BRB (pH 7.0) solution, the modified electrode exhibited an excellent venlafaxine oxidation behavior. The quantitative measurement of VEN was achieved using a simple, quick, and sensitive SWASV technique. The EIS and CV results revealed rapid charge transport through Co-Pd@Al₂O₃/GCE in comparison with the bare GCE. Under optimized conditions, the detection limit of VEN was estimated to be 1.86 pM. The slope of the plot of the peak potential as a function pH revealed the involvement of an equal number of electrons and protons in the oxidation mechanism of VEN. The modified electrode was found to possess the qualities of anti-interference ability, repeatability, reproducibility, and stability. Moreover, it showed a wide linearity range for VEN detection. The performance

of the designed sensor in aqueous and serum samples demonstrated the applicability of the adopted approach in the regular analysis of VEN samples. These figures of merit of the Co–Pd@Al₂O₃/GCE nanosensor for VEN detection point to its promising candidature for applications in clinical diagnostics.

Author Contributions: Conceptualization, S.S. and A.S.; methodology, S.S. and N.F.; formal analysis, S.S., N.F. and J.N.; investigation, S.S., J.N. and M.N.A.; resources, A.S. and I.S.; data curation, S.S., J.N. and I.S.; writing—original draft preparation, S.S.; writing—review and editing, A.S., I.S. and M.N.A.; visualization, S.S. and N.F.; supervision, A.S.; project administration, A.S. All authors have read and agreed to the published version of the manuscript.

Funding: This research received no external funding. The APC were kindly waived off by the journal.

Informed Consent Statement: Not applicable.

Data Availability Statement: Not applicable.

Acknowledgments: Authors gratefully acknowledge the support of Quaid-i-Azam University and the Higher Education Commission of Pakistan.

Conflicts of Interest: Authors declare no conflict of interest.

References

1. Manjula, N.; Pulikkutty, S.; Chen, T.W.; Chen, S.M.; Liu, X. Hexagon prism-shaped cerium ferrite embedded on GC electrode for electrochemical detection of antibiotic drug ofloxacin in biological sample. *Colloids Surf. A Physicochem. Eng. Asp.* **2021**, *627*, 127129. [[CrossRef](#)]
2. Aramesh Boroujeni, Z.; Aghbalaghi, Z.A. Electrochemical determination venlafaxine at NiO/GR nanocomposite modified carbon paste electrode. *Iran. J. Chem. Chem. Eng.* **2021**, *40*, 1042–1053.
3. Rezvani Jalal, N.; Mehrbod, P.; Shojaei, S.; Labouta, H.I.; Mokarram, P.; Afkhami, A.; Madrakian, T.; Los, M.J.; Schaafsma, D.; Giersig, M.; et al. Magnetic nanomaterials in microfluidic sensors for virus detection: A review. *ACS Appl. Nano Mater.* **2021**, *4*, 4307–4328. [[CrossRef](#)]
4. Maddah, B.; Cheraghveisi, M.; Najafi, M. Developing a modified electrode based on La³⁺/Co₃O₄ Nanocubes and its usage to electrochemical detection of venlafaxine. *Int. J. Environ. Anal. Chem.* **2020**, *100*, 121–133. [[CrossRef](#)]
5. El-Kashef, D.H.; Sharawy, M.H. Venlafaxine mitigates cisplatin-induced nephrotoxicity via down-regulating apoptotic pathway in rats. *Chem. Biol. Intract.* **2018**, *290*, 110–118. [[CrossRef](#)] [[PubMed](#)]
6. Thompson, W.A.; Arnold, V.I.; Vijayan, M.M. Venlafaxine in embryos stimulates neurogenesis and disrupts larval behavior in zebrafish. *Environ. Sci. Technol.* **2017**, *21*, 12889–12897. [[CrossRef](#)] [[PubMed](#)]
7. Parrott, J.L.; Metcalfe, C.D. Assessing the effects of the antidepressant venlafaxine to fathead minnows exposed to environmentally relevant concentrations over a full life cycle. *Environ. Pollut.* **2017**, *229*, 403–411. [[CrossRef](#)]
8. Zucker, I.; Mamane, H.; Riani, A.; Gozlan, I.; Avisar, D. Formation and degradation of N-oxide venlafaxine during ozonation and biological post-treatment. *Sci. Total Environ.* **2018**, *619*, 578–586. [[CrossRef](#)]
9. Fard, N.T.; Tadayon, F.; Panahi, H.A.; Moniri, E. The synthesis of functionalized graphene oxide by polyester dendrimer as a pH-sensitive nanocarrier for targeted delivery of venlafaxine hydrochloride: Central composite design optimization. *J. Mol. Liq.* **2022**, *349*, 118149. [[CrossRef](#)]
10. Norouzi, P.; Larijani, B.; Alizadeh, T.; Pourbasheer, E.; Aghazadeh, M.; Ganjali, M.R. Application of advanced electrochemical methods with nanomaterial-based electrodes as powerful tools for trace analysis of drugs and toxic compounds. *Curr. Anal. Chem.* **2019**, *2*, 143–151. [[CrossRef](#)]
11. Matoga, M.; Pehourcq, F.; Titier, K.; Dumora, F.; Jarry, C. Rapid high-performance liquid chromatographic measurement of venlafaxine and O-desmethylvenlafaxine in human plasma: Application to management of acute intoxications. *J. Chromatogr. B Biomed. Appl.* **2001**, *760*, 213–218. [[CrossRef](#)]
12. Mandrioli, R.; Mercolini, L.; Cesta, R.; Fanali, S.; Amore, M.; Raggi, M.A. Analysis of the second generation antidepressant venlafaxine and its main active metabolite O-desmethylvenlafaxine in human plasma by HPLC with spectrofluorimetric detection. *J. Chromatogr. B* **2007**, *856*, 88–94. [[CrossRef](#)]
13. Bhatt, J.; Jangid, A.; Venkatesh, G.; Subbaiah, G.; Singh, S. Liquid chromatography–tandem mass spectrometry (LC–MS–MS) method for simultaneous determination of venlafaxine and its active metabolite O-desmethyl venlafaxine in human plasma. *J. Chromatogr. B* **2005**, *829*, 75–81. [[CrossRef](#)]
14. Mastrogianni, O.; Theodoridis, G.; Spagou, K.; Violante, D.; Henriques, T.; Pouliopoulos, A.; Raikos, N. Determination of venlafaxine in post-mortem whole blood by HS-SPME and GC-NPD. *Forensic Sci. Int.* **2012**, *215*, 105–109. [[CrossRef](#)]
15. Madrakian, T.; Haryani, R.; Ahmadi, M.; Afkhami, A. Spectrofluorometric determination of venlafaxine in biological samples after selective extraction on the superparamagnetic surface molecularly imprinted nanoparticles. *Anal. Method.* **2015**, *7*, 428–435. [[CrossRef](#)]

16. Guo, C.; Xiao, Y. Negatively charged cyclodextrins: Synthesis and applications in chiral analysis—A review. *Carbohydr. Polym.* **2021**, *256*, 117517. [[CrossRef](#)]
17. Martins, F.C.; Pimenta, L.C.; De Souza, D. Antidepressants determination using an electroanalytical approach: A review of methods. *J. Pharm. Biomed. Anal.* **2021**, *206*, 114365. [[CrossRef](#)]
18. Mobin, S.M.; Sanghavi, B.J.; Srivastava, A.K.; Mathur, P.; Lahiri, G.K. Biomimetic sensor for certain phenols employing a copper (II) complex. *Anal. Chem.* **2010**, *82*, 5983–5992. [[CrossRef](#)]
19. Sanghavi, B.J.; Srivastava, A.K. Simultaneous voltammetric determination of acetaminophen, aspirin and caffeine using an in situ surfactant-modified multiwalled carbon nanotube paste electrode. *Electrochim. Acta.* **2010**, *55*, 8638–8648. [[CrossRef](#)]
20. Gadhari, N.S.; Sanghavi, B.J.; Karna, S.P.; Srivastava, A.K. Potentiometric stripping analysis of bismuth based on carbon paste electrode modified with cryptand [2.2.1] and multiwalled carbon nanotubes. *Electrochim. Acta* **2010**, *56*, 627–635. [[CrossRef](#)]
21. Görög, S. The changing face of pharmaceutical analysis. *Trends Anal. Chem.* **2007**, *26*, 12–17. [[CrossRef](#)]
22. Sanghavi, B.J.; Srivastava, A.K. Adsorptive stripping differential pulse voltammetric determination of venlafaxine and desvenlafaxine employing Nafion–carbon nanotube composite glassy carbon electrode. *Electrochim. Acta* **2011**, *56*, 4188–4196. [[CrossRef](#)]
23. Aftab, S.; Kurbanoglu, S.; Ozcelikay, G.; Bakirhan, N.K.; Shah, A.; Ozkan, S.A. Carbon quantum dots co-catalyzed with multiwalled carbon nanotubes and silver nanoparticles modified nanosensor for the electrochemical assay of anti-HIV drug Rilpivirine. *Sens. Actuators B Chem.* **2019**, *285*, 571–583. [[CrossRef](#)]
24. Zen, J.M.; Senthil Kumar, A.; Tsai, D.M. Recent updates of chemically modified electrodes in analytical chemistry. *Electroanalysis* **2003**, *15*, 1073–1087. [[CrossRef](#)]
25. Xu, J.; Tao, J.; Su, L.; Wang, J.; Jiao, T. A Critical Review of Carbon Quantum Dots: From Synthesis toward Applications in Electrochemical Biosensors for the Determination of a Depression-Related Neurotransmitter. *Materials* **2021**, *14*, 3987. [[CrossRef](#)]
26. Shah, A.; Akhtar, M.; Aftab, S.; Shah, A.H.; Kraatz, H.B. Gold copper alloy nanoparticles (Au–Cu NPs) modified electrode as an enhanced electrochemical sensing platform for the detection of persistent toxic organic pollutants. *Electrochim. Acta* **2017**, *241*, 281–290. [[CrossRef](#)]
27. Oyama, M. Recent nanoarchitectures in metal nanoparticle-modified electrodes for electroanalysis. *Anal. Sci.* **2010**, *26*, 1–12. [[CrossRef](#)]
28. Gao, J.; Fu, L.J.; Zhang, H.P.; Yang, L.C.; Wu, Y.P. Improving electrochemical performance of graphitic carbon in PC-based electrolyte by nano-TiO₂ coating. *Electrochim. Acta* **2008**, *53*, 2376–2379. [[CrossRef](#)]
29. Raj, N.; Crooks, R.M. Detection Efficiency of Ag Nanoparticle Labels for a Heart Failure Marker Using Linear and Square-Wave Anodic Stripping Voltammetry. *Biosensors* **2022**, *4*, 203. [[CrossRef](#)]
30. Xie, C.; Li, H.; Li, S.; Wu, J.; Zhang, Z. Surface molecular self assembly for organophosphate pesticide imprinting in electropolymerized poly (paminothiophenol) membranes on a gold nanoparticle modified glassy carbon electrode. *Anal. Chem.* **2010**, *82*, 241–249. [[CrossRef](#)]
31. Wen, X.; Fei, J.; Chen, X.; Yi, L.; Ge, F.; Huang, M. Electrochemical analysis of trifluralin using a nanostructuring electrode with multi-walled carbon nanotubes. *Environ. Pollut.* **2008**, *3*, 1015–1020. [[CrossRef](#)] [[PubMed](#)]
32. Uygun, Z.O.; Dilgin, Y. A novel impedimetric sensor based on molecularly imprinted polypyrrole modified pencil graphite electrode for trace level determination of chlorpyrifos. *Sens. Actuators B Chem.* **2013**, *188*, 78–84. [[CrossRef](#)]
33. Zhang, L.; Lee, K.; Zhang, J. Effect of synthetic reducing agents on morphology and ORR activity of carbon-supported nano-Pd–Co alloy electrocatalysts. *Electrochim. Acta* **2007**, *52*, 7964–7971. [[CrossRef](#)]
34. Welch, C.M.; Compton, R.G. The use of nanoparticles in electroanalysis: A review. *Anal. Bioanal. Chem.* **2006**, *384*, 601–619. [[CrossRef](#)]
35. Firdous, N.; Janjua, N.K. CoPt_x/γ-Al₂O₃ bimetallic nanoalloys as promising catalysts for hydrazine electrooxidation. *Heliyon* **2019**, *5*, e01380. [[CrossRef](#)]
36. Wang, D.; Li, Y. Bimetallic nanocrystals: Liquid-phase synthesis and catalytic applications. *Adv. Mater.* **2011**, *23*, 1044–1060. [[CrossRef](#)]
37. White, R.J.; Luque, R.; Budarin, V.L.; Clark, J.H.; Macquarrie, D.J. Supported metal nanoparticles on porous materials. *Chem. Soc. Rev.* **2009**, *38*, 481–494. [[CrossRef](#)]
38. Trueba, M.; Trasatti, S.P. γ-Alumina as a support for catalysts: A review of fundamental aspects. *Eur. J. Inorg. Chem.* **2005**, *2005*, 3393–3403. [[CrossRef](#)]
39. Windmiller, J.R.; Bandodkar, A.J.; Parkhomovsky, S.; Wang, J. Stamp transfer electrodes for electrochemical sensing on non-planar and oversized surfaces. *Analyst* **2012**, *137*, 1570–1575. [[CrossRef](#)]
40. Dong, S.; Kuwana, T. Activation of glassy carbon electrodes by dispersed metal oxide particles: I. ascorbic acid oxidation. *J. Electrochem. Soc.* **1984**, *131*, 813. [[CrossRef](#)]
41. Chowdhury, S.R.; Ghosh, S.; Bhattacharya, S.K. Enhanced and synergistic catalysis of one-pot synthesized palladium-nickel alloy nanoparticles for anodic oxidation of methanol in alkali. *Electrochim. Acta* **2017**, *250*, 124–134. [[CrossRef](#)]
42. Li, H.; Xie, C.; Li, S.; Xu, K. Electropolymerized molecular imprinting on gold nanoparticle-carbon nanotube modified electrode for electrochemical detection of triazophos. *Colloids Surf. B Biointerfaces* **2012**, *89*, 175–181. [[CrossRef](#)]
43. Dequaire, M.; Degrand, C.; Limoges, B. An electrochemical metalloimmunoassay based on a colloidal gold label. *Anal. Chem.* **2000**, *72*, 5521–5528. [[CrossRef](#)]

44. Tominaga, M.; Taema, Y.; Taniguchi, I. Electrocatalytic glucose oxidation at bimetallic gold–copper nanoparticle-modified carbon electrodes in alkaline solution. *J. Electroanal. Chem.* **2008**, *624*, 1–8. [[CrossRef](#)]
45. Dervisevic, M.; Dervisevic, E.; Çevik, E.; Şenel, M. Novel electrochemical xanthine biosensor based on chitosan–polypyrrole–gold nanoparticles hybrid bio-nanocomposite platform. *J. Food Drug Anal.* **2017**, *25*, 510–519. [[CrossRef](#)]
46. Hosseini, M.; Jafarian, T.; Rostami, M.; Gopal, F. A low cost and highly active non-noble alloy electrocatalyst for hydrazine oxidation based on nickel ternary alloy at the surface of graphite electrode. *J. Electroanal. Chem.* **2016**, *763*, 134–140.
47. Tamašauskaitė-Tamašiūnaitė, L.; Rakauskas, J.; Balčiūnaitė, A.; Zabelaitė, A.; Vaičiūnienė, J.; Selskis, A.; Norkus, E. Gold–nickel/titania nanotubes as electrocatalysts for hydrazine oxidation. *J. Power Sources* **2014**, *272*, 362–370. [[CrossRef](#)]
48. Jiang, S.; Ma, Y.; Jian, G.; Tao, H.; Wang, X.; Fan, Y.; Chen, Y. Facile construction of Pt–Co/CN_x nanotube electrocatalysts and their application to the oxygen reduction reaction. *Adv. Mater.* **2009**, *21*, 4953–4956. [[CrossRef](#)]
49. Jahani, P.M.; Javar, H.A.; Mahmoudi-Moghaddam, H. A new electrochemical sensor based on Europium-doped NiO nanocomposite for detection of venlafaxine. *Measurement* **2021**, *173*, 108616. [[CrossRef](#)]
50. Zaimbashi, R.; Mostafavi, A.; Shamspur, T. ZnO nanoflower based electrochemical sensor for the selective determination of venlafaxine. *J. Iran. Chem. Soc.* **2021**, *19*, 1329–1337. [[CrossRef](#)]
51. Ibrahim, H.; Temerk, Y. Novel sensor for sensitive electrochemical determination of luteolin based on In₂O₃ nanoparticles modified glassy carbon paste electrode. *Sens. Actuators B Chem.* **2015**, *206*, 744–752. [[CrossRef](#)]
52. Beitollahi, H.; Jahani, S.; Tajik, S.; Ganjali, M.R.; Faridbod, F.; Alizadeh, T. Voltammetric determination of venlafaxine as an antidepressant drug employing Gd₂O₃ nanoparticles graphite screen printed electrode. *J. Rare Earths* **2019**, *37*, 322–328. [[CrossRef](#)]
53. Parida, K.M.; Pradhan, A.C.; Das, J.; Sahu, N. Synthesis and characterization of nano-sized porous gamma-alumina by control precipitation method. *Mater. Chem. Phys.* **2009**, *113*, 244–248. [[CrossRef](#)]
54. Jiang, Y.; Kang, Q.; Zhang, J.; Dai, H.B.; Wang, P. High-performance nickel–platinum nanocatalyst supported on mesoporous alumina for hydrogen generation from hydrous hydrazine. *J. Power Sources* **2015**, *273*, 554–560. [[CrossRef](#)]
55. Wang, Z.; Xu, X.; Liu, Z.; Zhang, D.; Yuan, J.; Liu, J. Multifunctional Metal Phosphides as Superior Host Materials for Advanced Lithium–Sulfur Batteries. *Eur. J. Chem.* **2021**, *27*, 13494–13512. [[CrossRef](#)]
56. Naik, B.; Prasad, V.S.; Ghosh, N.N. Development of a simple aqueous solution based chemical method for synthesis of mesoporous γ -alumina powders with disordered pore structure. *J. Porous Mater.* **2010**, *17*, 115–121. [[CrossRef](#)]
57. Rudaz, S.; Stella, C.; Balant-Gorgia, A.E.; Fanali, S.; Veuthey, J.L. Simultaneous stereoselective analysis of venlafaxine and O-desmethylvenlafaxine enantiomers in clinical samples by capillary electrophoresis using charged cyclodextrins. *J. Pharm. Biomed. Anal.* **2000**, *23*, 107–115. [[CrossRef](#)]
58. Vaze, V.D.; Srivastava, A.K. Electrochemical behavior of folic acid at calixarene based chemically modified electrodes and its determination by adsorptive stripping voltammetry. *Electrochim. Acta* **2007**, *53*, 1713. [[CrossRef](#)]
59. Toan, T.T.T.; Dao, A.Q.; Vasseghian, Y. A state-of-the-art review on the nanomaterial-based sensor for detection of venlafaxine. *Chemosphere* **2022**, *297*, 134116.
60. Morais, S.; Ryckaert, C.P.; Delerue-Matos, C. Adsorptive stripping voltammetric determination of venlafaxine in urine with a mercury film microelectrode. *Anal. Lett.* **2003**, *36*, 2515–2526. [[CrossRef](#)]
61. Khalilzadeh, M.A.; Tajik, S.; Beitollahi, H.; Venditti, R.A. Green synthesis of magnetic nanocomposite with iron oxide deposited on cellulose nanocrystals with copper (Fe₃O₄@CNC/Cu): Investigation of catalytic activity for the development of a venlafaxine electrochemical sensor. *Ind. Eng. Chem. Res.* **2020**, *59*, 4219–4228. [[CrossRef](#)]
62. Eslami, E.; Farjami, F. Voltammetric determination of venlafaxine by using multiwalled carbon nanotube-ionic liquid composite electrode. *J. Appl. Chem. Res.* **2018**, *12*, 42–52.
63. Ding, L.; Li, L.; You, W.; Gao, Z.N.; Yang, T.L. Electrocatalytic oxidation of venlafaxine at a multiwall carbon nanotubes-ionic liquid gel modified glassy carbon electrode and its electrochemical determination. *Croat. Chem. Acta* **2015**, *88*, 81–87. [[CrossRef](#)]
64. Senturk, H.; Karadeniz, H.; Erdem, A. Recent Applications of Nanomaterials Based on Electrochemical Drug Analysis. *Curr. Org. Chem.* **2021**, *17*, 1215–1228. [[CrossRef](#)]